NbCl$_5$ and CrCl$_3$ catalysts effect on synthesis and hydrogen storage performance of Mg–Ni–NiO composites

QI WAN, PING LI*, **TENG WANG, XUANHUI QU, FUQIANG ZHAI, ALEX A VOLINSKY[†] and PHILIP J LOGAN[†]**

School of Material Science and Engineering, University of Science and Technology Beijing, Beijing 100083, China
[†]Department of Mechanical Engineering, University of South Florida, Tampa, FL 33620, USA

Abstract. Two kinds of novel materials, Mg–1·6 mol%Ni–0·4 mol%NiO–2 mol%MCl (MCl = NbCl$_5$, CrCl$_3$), along with Mg–1·6 mol%Ni–0·4 mol%NiO for comparison, were examined for their potential use in hydrogen storage applications, having been fabricated via cryomilling. The effects of NbCl$_5$ and CrCl$_3$ on hydrogen storage performance were investigated. A microstructure analysis showed that besides the main Mg and Ni phases, NiO and Mg$_2$Ni phases were present in all samples. MgCl$_2$ was only found in halide-doped samples and NbO was only found in NbCl$_5$-doped samples after ball milling. The particle size decreased significantly after 7 h of cryomilling. MgH$_2$, Mg$_2$NiH$_4$ and Mg$_2$NiH$_{0.3}$ were present in all the samples, while NbH$_2$ was only observed in the NbCl$_5$-doped sample after absorption. The NbCl$_5$-containing composite exhibited a low onset absorption temperature of 323 K, which was 10 K lower than that of the no-halide doped catalyst. It absorbed 5·32 wt% of hydrogen in 370 s at 623 K under 4 MPa hydrogen pressure and can absorb 90% of its full hydrogen capacity in 50 s. Having an onset desorption temperature of 483 K in vacuum, the NbCl$_5$-containing composite desorbed hydrogen faster than the no-halide doped sample. The hydriding–dehydriding kinetics performance of the CrCl$_3$-doped sample did not improve, but it did exhibit a lower onset desorption temperature of 543 K under 0·1 MPa, which was 20 K lower than that of the no-halide doped sample. NbO, NiO and NbH$_2$ played important roles in improving absorption and desorption performances.

Keywords. Hydrogen storage; Mg-based materials; hydrogen storage performance; catalyst.

1. Introduction

There is a great interest in developing suitable materials for hydrogen storage application. A number of materials ranging from interstitial metal hydrides to complex hydrides such as alanates, borohydrides and imides have been extensively studied (Ismail *et al* 2011; Varin and Jang 2011; Li *et al* 2011; Varin and Parviz 2012; Jiang *et al* 2012). Interstitial metal hydrides such as LaNi$_5$H$_6$ can absorb hydrogen rapidly and reversibly at moderate temperature and pressures, but hydrogen storage capacity limits their potential for hydrogen storage. Complex hydrides such as alanates have very high hydrogen storage capacities but it is difficult to absorb hydrogen. LiBH$_4$ and LiNH$_2$ also have very high hydrogen storage capacities but desorption is often accompanied by the byproduct such as B$_2$H$_6$ and NH$_3$ (Sakintuna *et al* 2007; Hausdorf *et al* 2008; Li *et al* 2011; Zhai *et al* 2012).

Magnesium hydride is an attractive material for hydrogen storage because, it can reversibly store up to 7·6 wt% hydrogen and desorption occurs via a simple one-step process with one byproduct. Unfortunately, due to its poor activation, kinetic performance and high dehydrogenation tempera-

ture, it cannot be practically used yet (Berry *et al* 1995; Tonus *et al* 2009; Fuster *et al* 2009; Principi *et al* 2009; Barbir 2009; Neef 2009; Jain 2009; Fan *et al* 2010; Jain *et al* 2010). To solve these problems, synthesis technology has to be improved. Ball milling is an effective method to improve the activation and hydrogen performance of Mg by transforming its structure (Kwon *et al* 2008). In addition, substances or compounds can be added to Mg for better hydrogen storage performance. Mg provides high hydrogen storage capability, while additives act as catalysts to improve the rate of hydrogen absorption and desorption and decrease the hydrogen storage temperature. Among these additives, some transitional metals (Barkhordarian *et al* 2003; Czujko *et al* 2006), their oxides (Mao *et al* 2010) and halides (Ma *et al* 2009) provide good catalytic effects. Since a single additive does not provide enough catalytic power (Kalisvaart *et al* 2010), several additives working together improve the materials' hydrogen storage abilities, with promising results (Hong *et al* 2008). Adding binary catalysts to Mg is a hot topic, while ternary catalysts in Mg are rarely reported. It has been shown that Mg-based hydrogen storage materials, prepared with cryomilling, have excellent properties (Xiong *et al* 2009). In this paper, two novel materials, Mg–1·6 mol%Ni–0·4 mol%NiO–2 mol%MCl (MCl = NbCl$_5$, CrCl$_3$), have been fabricated by mechanical milling,

---

*For correspondence (ustbliping@163.com)

at cryogenic temperatures (cryomilling). Mg–1·6 mol%Ni–0·4 mol%NiO was prepared for comparison under the same conditions. This paper describes the synthesis of Mg-based hydrogen storage materials and analyses the effects of $NbCl_5$ and $CrCl_3$ on its hydriding–dehydriding kinetics performance.

2. Experimental

The starting materials were powders of pure Mg ($\geq$99·9%, 74 μm), NiO ($\geq$99·9%, 10 μm), Ni ($\geq$99·7%, 3 μm) and MCl ($NbCl_5$, $CrCl_3$) ($\geq$99·9%, 3 μm), used without further purification. These powders were mixed to obtain Mg–1·6 mol%Ni–0·4 mol%NiO–2 mol%MCl (MCl = $NbCl_5$, $CrCl_3$) (MCl represents $MbCl_5$ or $CrCl_3$) composition. The mixture was placed into a stainless steel container. The ball diameter was 5 mm with the ball-to-powder mass ratio in the pot of 20:1. The milling was undertaken on QM–ISP planetary ball mill (manufactured by Nanjing University, China) with a fixed 350 rpm rotation speed for 7 h at cryogenic temperature (238 $\pm$ 5 K). Handling, weighting, loading of the samples and ball milling were performed in air without any protective atmosphere.

The particle size of the powders were measured by using a laser particle size analyser (Japan, 0·1–1000 μm). Structure and morphology of the powders were characterized by X-ray diffraction (10 s per 0·02° 2θ step) using Philips PW 1710 diffractometer with CuKα radiation ($\lambda = 0$·15405 nm) and LEO-1450 scanning electron microscope (SEM), respectively. Dehydriding–hydriding properties of the samples were examined by using a pressure–composition–temperature apparatus (manufactured by Beijing Nonferrous Metal Research Institution, China).

3. Results and discussion

3.1 *XRD analysis*

Figure 1 shows XRD patterns of Mg–1·6 mol%Ni–0·4 mol%NiO–2 mol%MCl (MCl = $NbCl_5$, $CrCl_3$) and Mg–1·6 mol%Ni–0·4 mol%NiO, after having been milled for 7 h before and after absorption. It can be seen from figure 1(a) that Mg, Ni, NiO reflections, with a small Mg_2Ni (JCPDS# 65-3621) reflection, are observed in all the samples. New NbO and $MgCl_2$ (JCPDS# 25-1156) phases appear in the milled Mg–1·6 mol%Ni–0·4 mol%NiO–2 mol% $NbCl_5$ sample, new phase $MgCl_2$ is observed but $CrCl_3$ still exists in the milled Mg–1·6 mol%Ni–0·4 mol%NiO–2 mol%$CrCl_3$ sample. Figure 1(b) indicates that Mg, MgH_2, Ni, MgO, small amounts of the Mg_2NiH_4 and $Mg_2NiH_{0·3}$ phases are observed in all of the absorption samples. The amount of NiO is too small to be detected, while the $MgCl_2$ and NbO phases are found in all doped samples, with the NbH_2 being found only in the $NbCl_5$-doped sample.

3.2 *Size and morphology analysis*

Figure 2 shows SEM images of the three samples and table 1 lists their particles size. The images indicate that the average size of the $NbCl_5$ and $CrCl_3$-doped samples are smaller than 20 and 30 μm, respectively. The no-halide catalyst sample is between 50 and 60 μm. Table 1 shows that the particle size of most of the $NbCl_5$ and $CrCl_3$-doped samples are about 12 and 23 μm, respectively. However, particle size of the no-halide catalyst sample is three times and 1·5 times larger than those of the $NbCl_5$ and $CrCl_3$-doped samples, respectively. Although the process of fabricating all the samples is the same, the particle size differs and the reason
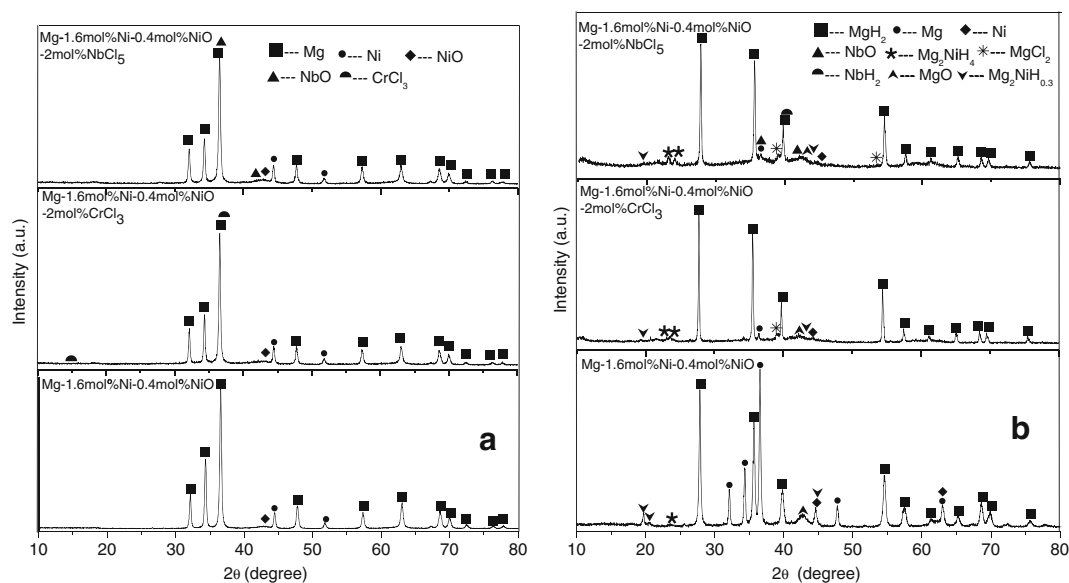
Figure 1. XRD patterns of Mg–1·6 mol%Ni–0·4 mol%NiO–2 mol%MCl (MCl = $NbCl_5$,$CrCl_3$) and Mg–1·6 mol%Ni–0·4 mol%NiO milled for 7 h: (**a**) before and (**b**) after hydrogenation.
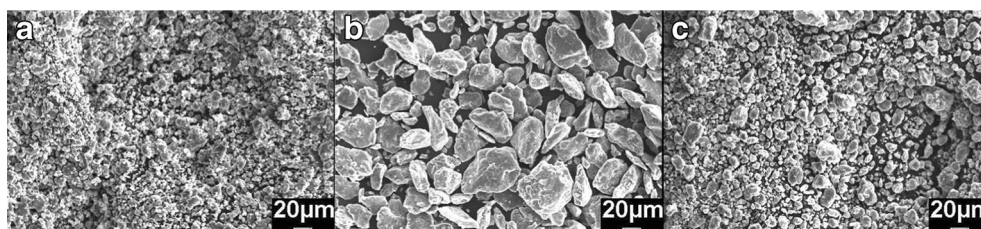
Figure 2. SEM images of Mg–1·6 mol%Ni–0·4 mol%NiO–2 mol%MCl: (**a**) MCl = NbCl₅; (**b**) no-halide catalyst; (**c**) MCl = CrCl₃ milled for 7 h.
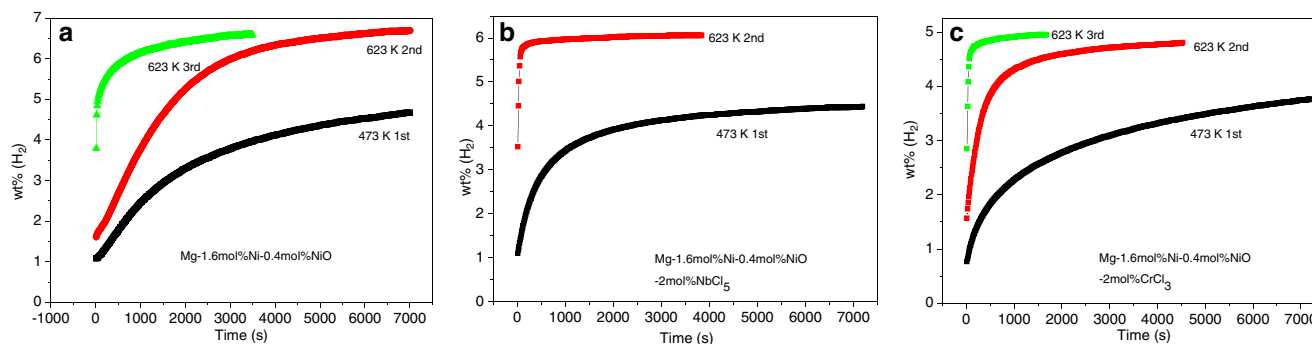
Figure 3. Activation curves of Mg–1·6 mol%Ni–0·4 mol%NiO–2 mol%MCl (MX = NbCl₅, CrCl₃) and Mg–1·6 mol%Ni–0·4 mol%NiO milled for 7 h.

Table 1. Particle size of Mg–1·6 mol%Ni–0·4 mol%NiO–2 mol%MCl (MCl = NbCl₅, CrCl₃) and Mg–1·6 mol%Ni–0·4 mol%NiO milled for 7 h.

Samples/items	Shape factor	X50/μm	SSA/(m^2/cm^3)	Normal distribution/σ
Mg–1·6 mol%Ni–0·4 mol%NiO–2 mol%NbCl₅	1·000	12·589	0·785	1·978
Mg–1·6 mol%Ni–0·4 mol%NiO	1·000	35·865	0·207	1·610
Mg–1·6 mol%Ni–0·4 mol%NiO–2 mol%CrCl₃	1·000	22·865	0·357	1·810

Notice: shape factor: the parameter was decided by the shape of particles, if SF = 1·000, it is sphere; X50: the diameter of particles, when the cumulative distribution equates 50%; SSA: superficial area per volume; normal distribution: standard deviation of normal function; the particles size distributes in a wide range, when the value is big; the particles size distributes in a narrow range, when the value is small.

may be that halide is hygroscopic. As a result, low temperature ball milling caused moisture within the halide to freeze and turn into ice, which, in turn, acted as a lubricant. This caused the powders not to stick to the wall of the jar, which can be seen in the experiment, thereby improving the process of efficiency.

3.3 *Hydrogen storage performance*

3.3a *Activation performance*: Figure 3 shows activation curves of all samples. In this work, the design activation procedure is as follows: (i) absorb hydrogen at 473 K; (ii) increase the temperature to 623 K to release the hydrogen and (iii) further activate at 623 K. It can be seen from figure 3 that all the samples have an excellent activation performance.

They absorb hydrogen during first time of activation at 473 K and after one or two activations, the samples achieve optimal absorption/desorption properties. The outstanding performance is attributed to ball milling at low temperature. At cryogenic temperatures, oxygen is less chemically active, thereby preventing the formation of MgO on the surface of the powder particles, if the amount of MgO decreases, the sample can be activated easily and can absorb more hydrogen, as Mg is the absorption phase. Among the three samples, the NbCl₅-doped sample has an exceedingly fast hydrogenation rate, proving that at least some of the NbCl₅ reacts with H₂ and forms NbH₂, thereby promoting the first activation process. CrCl₃-doped sample has the slowest hydrogenation rate, possibly because CrCl₃ does not react with other components and cannot form new phase which improves the

activation performance at the same time, the CrCl$_3$ cannot facilitate activation process alone.

3.3b *Onset temperature of absorption and desorption*: Figure 4 shows hydrogen absorption and desorption curves and the absorption and desorption rate curves for the three samples at 2·5 K/min heating rate. The initial hydrogen

absorption pressure is 4 MPa and the pressure of desorption is 0·1 MPa or vacuum.

It can be seen from figure 4(a), that the hydrogenation rate curves have two slopes: (i) as the physical hydrogen absorption process saturates, for which the hydrogen absorption rate is very fast, but then quickly declines as the rate descends to its lowest point and (ii) as the rate goes up, the hydride
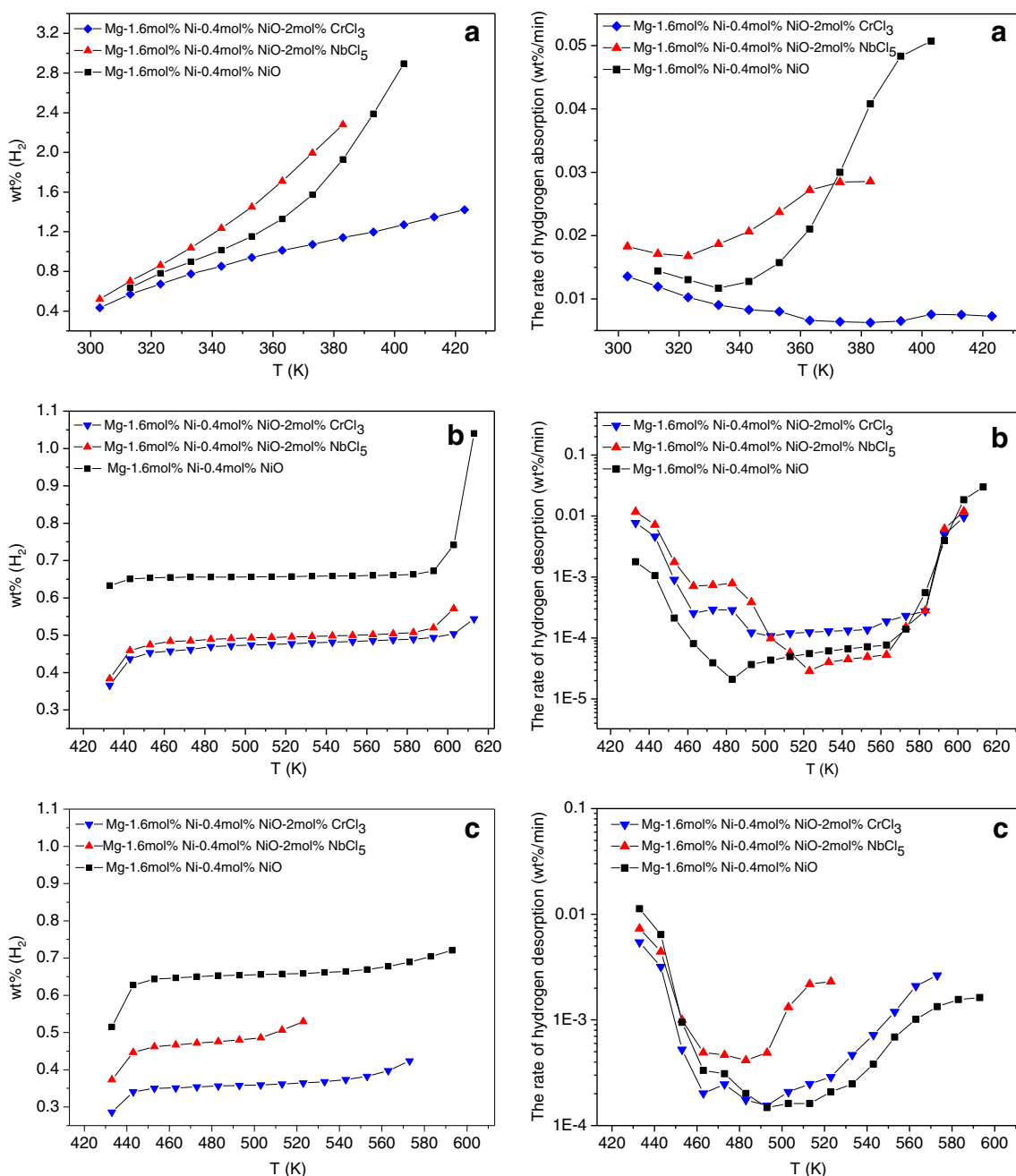
Figure 4. H$_2$ absorption and desorption curves and absorption and desorption rate curves of Mg–1·6 mol%Ni–0·4 mol%NiO–2 mol%MCl (MCl = NbCl$_5$, CrCl$_3$) and Mg–1·6 mol%Ni–0·4 mol%NiO milled for 7 h, under the temperature increasing rate of 2·5 K/min: (**a**) absorption curves; (**b**) desorption curves under 0·1 MPa; (**c**) desorption curves in vacuum.

forms. We define the breakpoint of the hydrogenation rate as the onset hydrogenation temperature.

Figure 4(a) shows that $CrCl_3$-doped and no-halide catalyst samples have the same 333 K onset of hydrogenation temperature, while the $NbCl_5$-doped sample has an onset hydrogenation temperature of 323 K. This result indicates that $NbCl_5$ doping can lower the onset of hydrogenation temperature of the sample. XRD patterns (figure 2) show that NbO only exists in the $NbCl_5$-doped sample and therefore, must play main role in reducing the onset of hydrogenation temperature.

Figure 4(b, c) shows that dehydrogenation rate curves have three branches: (i) the hydrogen desorption rate is very fast and drops extremely fast, which is defined as the physical hydrogen desorption process, (ii) the rate is very low and tends to stabilize, being sustained until the hydride begins to release and (iii) the hydride starts to decompose, at which point the rate begins to soar. We define this turning point as

the onset of dehydrogenation temperature. As can be seen, the NbO phase is probably not beneficial in decreasing the onset temperature of dehydrogenation.

Figure 4(b) shows that under 0·1 MPa pressure, the onset of dehydrogenation temperature of the no-halide catalyst, $CrCl_3$-doped and $NbCl_5$-doped samples are 563, 573 and 543 K, respectively. Combined with XRD patterns seen in figure 2, it can be stated that $CrCl_3$ doping can promote reduction of the onset of dehydrogenation temperature under the 0·1 MPa pressure. Transition metal halide can decline the onset of dehydrogenation temperature of Mg (Jin *et al* 2007; Malka *et al* 2010).

Figure 4(c) reveals that no-halide catalyst and $CrCl_3$-doped samples have the same 493 K onset dehydrogenation temperature in vacuum. The $NbCl_5$-doped samples, however, have 483 K onset dehydrogenation temperature in vacuum and desorb hydrogen faster than the other two.

Drop of the onset dehydrogenation partially attributes to the decline of particle sizes, it can be seen from table 1, that particle sizes of halide doped samples are smaller than that of no-halide doped sample, this is in accord with the work reported (Aguey-Zinsou and Ares-Fernández 2008; Kalidindi and Jagirdar 2009).

3.3c *Kinetics performance*: Figure 5 shows absorption kinetics curves of the three samples at 623 K. The hydrogen storage capacity of no-halide catalyst, the $NbCl_5$-doped and the $CrCl_3$-doped samples are 6·02, 5·32 and 4·40 wt% at 623 K in 1900, 370 and 670 s, respectively. 90% of the full capacity is reached in 200, 40 and 50 s, respectively. Taking the average rate (wt%/min) of reaching 90% of the full capacity, for comparison purposes, following result is obtained $NbCl_5$-doped (5·85)>$CrCl_3$-doped (4·84)>no-halide catalyst (1·46).

The above results show that hydrogenation rate can be remarkably promoted by adding ternary catalysts. Combined with the results from XRD patterns (figure 2), it can

Figure 5. H_2 absorption curves at 623 K under 4 MPa hydrogen pressure for Mg–1·6 mol%Ni–0·4 mol%NiO–2 mol%MCl (MCl = $NbCl_5$, $CrCl_3$) and Mg–1·6 mol%Ni–0·4 mol% NiO milled for 7 h.
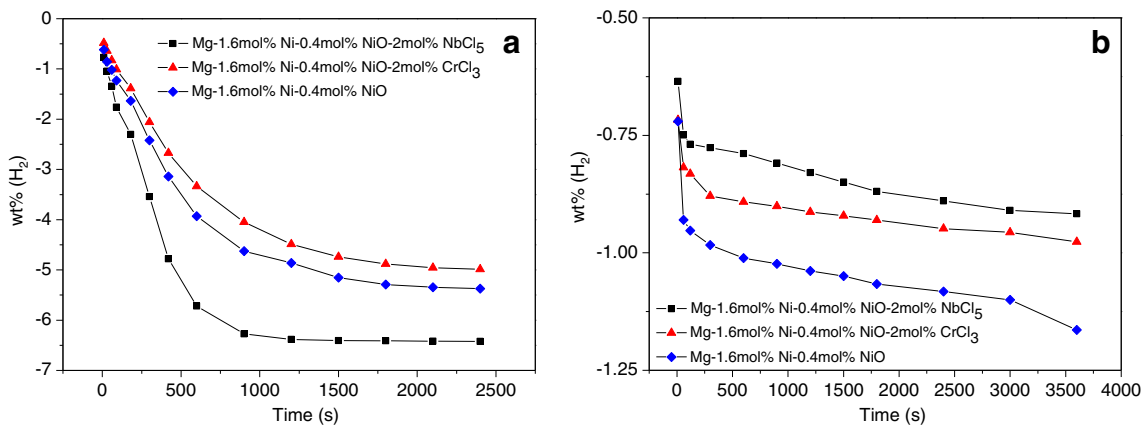
Figure 6. H_2 desorption curves under different conditions of Mg–1·6 mol%Ni–0·4 mol%NiO–2 mol% MCl (MCl = $NbCl_5$, $CrCl_3$) and Mg–1·6 mol%Ni–0·4 mol%NiO milled for 7 h: (**a**) desorption at 623 K under 0·1 MPa and (**b**) desorption at 523 K in vacuum.

be concluded that NbO ameliorates the absorption kinetics performance of the material.

All of the samples can start absorbing hydrogen at about 572 K under 0·1 MPa of pressure and at 493 K in vacuum. The absorption kinetics across all of the samples, at 623 K under 0·1 MPa of pressure and at 523 K in vacuum, were investigated. Figure 6 shows the desorption curves.

The figure indicates that the desorption kinetics of all of the samples are excellent at 623 K under 0·1 MPa of pressure. The time for releasing 80% of full hydrogen storage capacity of the no-halide catalyst, the NbCl$_5$-doped and the CrCl$_3$-doped samples are 550, 1000 and 900 s, respectively. Taking the average rate of releasing 80% of full capacity, for comparison purposes, provides the following result: no-halide catalyst (0·59)>CrCl$_3$-doped (0·28)>NbCl$_5$-doped (0·26).

Desorption performance of all of the samples is relatively erratic. The no-halide doped, the NbCl$_5$-doped sample and the CrCl$_3$-doped sample can desorb 0·92, 1·16 and 0·98 wt% of hydrogen, respectively at a temperature of 523 K, under vacuum in 3600 s. Figure 6(b) shows that NbCl$_5$-doped sample has two clear branches: (i) the fast branch and (ii) the slow branch. XRD pattern shows that NbH$_2$ phase forms in the NbCl$_5$-doped sample. Considering the instability of NbH$_2$, reaction (i) happens in the first stage, where the desorption rate is very fast.

$$2NbH_2 \rightarrow 2NbH + H_2. \tag{1}$$

When reaction (1) happens, a channel for diffusion is formed in the sample. Since the hydrogen in Mg$_2$NiH$_4$ and MgH$_2$ phases can be desorbed more easily through the channel, the desorption rate of the first stage is, therefore, faster than that found in the second stage.

4. Conclusions

(I) By doping Mg–1·6 mol%Ni–0·4 mol%NiO with NbCl$_5$ and CrCl$_3$, using the cryomilling technology, promising results were obtained. First, the Mg-based hydrogen storage materials fabricated by cryomilling have an outstanding activation performance. They can absorb hydrogen at 473 K before being activated at a higher temperature. Specifically, the NbCl$_5$-doped sample can absorb more than 4·4 wt% of hydrogen at 473 K during the first activation process. Second, some of the hydrogen storage properties of the materials were remarkably improved by the addition of NbCl$_5$ and CrCl$_3$ catalysts.

(II) In regard to the NbCl$_5$-doped sample, the onset absorption temperature declined to 323 K and the absorption/desorption kinetics performance was substantially improved. MgCl$_2$ phases were observed in the CrCl$_3$-doped sample after ball milling. No new phase was observed after the desorption. It can be concluded that CrCl$_3$ decreased the onset desorption temperature of CrCl$_3$-doped sample, under 0·1 MPa of pressure.

References

Aguey-Zinsou K-F and Ares-Fernández J-R 2008 *Chem. Mater.* **20** 376

Barbir F 2009 *Energy* **34** 308

Barkhordarian G, Klassen T and Bormann R 2003 *Scr. Mater.* **49** 213

Berry G D, Pasternak A D, Rambach G D, Smith J R and Schock R N 1995 *Energy* **21** 289

Czujko T, Varin R A, Chiu C and Wronski Z 2006 *J. Alloys Compd* **414** 240

Fan M Q, Liu S S, Zhang Y, Zhang J, Sun L X and Xu F 2010 *Energy* **35** 3417

Fuster V, Urretavizcaya G and Castro F J 2009 *J. Alloys Compd* **481** 673

Hausdorf S, Balitalow F, Wolf G and Mertens F 2008 *Int. J. Hydrogen Energy* **33** 608

Hong S H, Na Y S, Kwon S N, Bae J S and Song M Y 2008 *J. Alloys Compd* **465** 512

Ismail M, Zhao Y, Yu X B, Nevirkovets I P and Dou S X 2011 *J. Alloys Compd* **36** 8327

Jain I P 2009 *Int. J. Hydrogen Energy* **34** 7368

Jain I P, Chhagan Lal and Ankur Jain 2010 *Int. J. Hydrogen Energy* **35** 5133

Jiang Kun, Xiao Xuezhang, Lixin Chen, Han Leyuan, Shouquan Li and Hongwei Ge 2012 *J. Alloys Compd* **539** 103

Jin Seon-Ah, Shim Jae-Hyeok, Cho Young Whan and Yi Kyung-Woo 2007 *J. Power Sources* **172** 859

Kalidindi Suresh Babu and Jagirdar Balaji R 2009 *Inorg. Chem.* **48** 4524

Kalisvaart W P, Harrower C T, Haagsma J, Zahiri B, Luber E J and Ophus C 2010 *Int. J. Hydrogen Energy* **35** 2091

Kwon S N, Baek S H, Mumm D R, Hong S H and Song M Y 2008 *Int. J. Hydrogen Energy* **33** 4586

Li C, Peng P, Zhou D W and Wan L 2011 *Int. J. Hydrogen Energy* **36** 14512

Ma L P, Kang X D, Dai H B, Liang Y, Fang Z Z, Wang P J and Cheng H M 2009 *Acta Mater.* **57** 2250

Malka I E, Czujko T and Bystrzycki J 2010 *Int. J. Hydrogen Energy* **25** 1706

Mao J, Guo Z, Yu X, Liu H, Wu Z and Ni J 2010 *Int. J. Hydrogen Energy* **35** 4569

Neef H J 2009 *Energy* **34** 327

Principi G, Agresti F, Massalena A and Russo S L 2009 *Energy* **34** 2087

Sakintuna B, Lamari-Darkrim F and Hirscher M 2007 *Int. J. Hydrogen Energy* **32** 1121

Tonus F, Fuster V, Urretavizcaya G, Castro F J and Bobet J L 2009 *Int. J. Hydrogen Energy* **34** 3404

Varin R A and Jang M 2011 *J. Alloys Compd* **509** 7134

Varin R A and Parviz R 2012 *Int. J. Hydrogen Energy* **37** 9088

Xiong W, Li P, Xie D H, Zheng X P, Zheng C X and Qu X H 2009 *Rare Metal Mat. Eng.* **38** 365

Zhai Fuqiang *et al* 2012 *J. Phys. Chem. C* **116** 11939